Carbohydrate Polymers 106 (2014) 422–431

Contents lists available at ScienceDirect

Carbohydrate Polymers

journal homepage: www.elsevier.com/locate/carbpol

Azo dye/cyclodextrin: New findings of identical nanorods through 2:2 inclusion complexes

N. Rajendiran*, R.K. Sankaranarayanan

Department of Chemistry, Annamalai University, Annamalai Nagar 608 002, India

ARTICLE INFO

Article history:
Received 2 September 2013
Received in revised form 5 January 2014
Accepted 8 January 2014
Available online 21 January 2014

Keywords:
Cyclodextrin
Azo dyes
Inclusion complex
Self-assembly
Nanorod
Molecular modeling

ABSTRACT

Inclusion complexation behavior of 4-aminoazobenzene (AAB) and 4-amino-2,3′-dimethyl azobenzene (GBC, fast grant GBC) with α- and β-cyclodextrins (α-CD, β-CD) is analyzed by scanning electron microscope, transmission electron microscope, Fourier transform infrared spectroscopy, differential scanning calorimetry, powder X-ray diffraction, and proton nuclear magnetic resonance spectroscopy techniques. Transmission electron microscope analysis suggests that identical nanorods formed in AAB/CD inclusion complexes while different dimension nanostructures were observed in GBC/CD inclusion complexes. The nanostructures confirmed that the ratio of 2:2 (guest:host) inclusion complex has been developed to a miniature nanorod. Nanosecond time-resolved fluorescence studies indicated that AAB/GBC have fast life time in water, whereas slow life time in CDs corresponds to a higher-order structure of 2:2 complexes. Thermodynamic parameters and binding affinity of the inclusion complex formation were determined and discussed. van der Waals interactions are mostly responsible for enthalpy-driven complex formation of AAB and GBC with cyclodextrins.

1. Introduction

Cyclodextrin (CD) is a cyclic oligomer of α-D-glucose obtained by the action of certain enzymes on starch (Szejtli, 1998). In general CDs have shallow truncated cones; these carbohydrates present a hydrophobic cavity, whose size depends on the number of basic glucose units and two different rims, a wider (named head, H) having all secondary hydroxyl groups and a narrower (named tail, T) having all primary hydroxyl groups. The application of CD in chemistry is strongly associated to its ability to form inclusion complexes with a variety of guest molecules basically in aqueous solutions (Anconi, Nascimento, De Almeida, & Dos Santos, 2012; Connors, 1997). Because of CDs notable structure, CDs have also been used as a cyclic component in the assembly of supramolecular architectures (Harada, 2001). In supramolecular field, the cyclodextrins (CDs) are perfect host system for studying nano- and micro-structures through self-assembly of inclusion complexes. Mainly four models are responsible to form the linear type of nanostructures, head to head, tail to tail, head to tail and secondary self-assembly into stack way layer by layer arrangement. The CD nanorods form their secondary assembly through the hydrogen bonding between CDs (Miyake et al., 2003; Wu, Shen, & He, 2006). The hydrogen bond between the OH groups present along the rim of the CD is also an essential driving force leading to the formation of stable inclusion complex and nanostructure (Anconi et al., 2012; Ceccato, Lo Nostro, & Baglioni, 1997).

The application of molecular modeling techniques (Mohsen & Mina, 2009; Sherrod, 1992; VD'Souza & Lipkowitz, 1998) can help reinforce experimental results, such as stoichiometry, geometry and thermodynamics parameters accompanying the complexation process, and they also provide information on the driving forces responsible for such processes (Madrid, Mendicuti, & Mattice, 1998; Madrid, Pozuelo, Mendicuti, & Mattice, 1997). Further, molecular modeling studies on 1:1 inclusion complexes (Madrid et al., 1997) demonstrated that the formation of both inclusion complexes was complimentary with the nonbonded van der Waals interactions as the major participation to the stabilization. Moreover we merged the experimental and molecular modeling analysis leads to successful consequences in designing structure, energetic, enthalpy and entropy difficulties (Antony Muthu Prabhu, Sankaranarayanan, Venkatesh, & Rajendiran, 2012; Rajendiran & Siva, 2014; Sivasankar, Antony Muthu Prabhu, Karthick, & Rajendiran, 2012). We reported self-assembly of nanorod formation through the inclusion complex, nanorod formation mechanism was proposed based on the molecular modeling studies (Sankaranarayanan & Rajendiran, 2013).

In this study, the formation of identical nanorods between α-CD and β-CD with 4-aminoazobenzene (AAB) and 2,3-dimethyl-4-aminoazobenzene (GBC, fast grant GBC) molecules was discussed (Fig. 1). The formation of the nanorods layer by layer (LbL)

* Corresponding author. Tel.: +91 94866 28800; fax: +91 4144 238080.
E-mail address: drrajendiran@rediffmail.com (N. Rajendiran).

0144-8617/$ – see front matter © 2014 Elsevier Ltd. All rights reserved.
http://dx.doi.org/10.1016/j.carbpol.2014.01.030

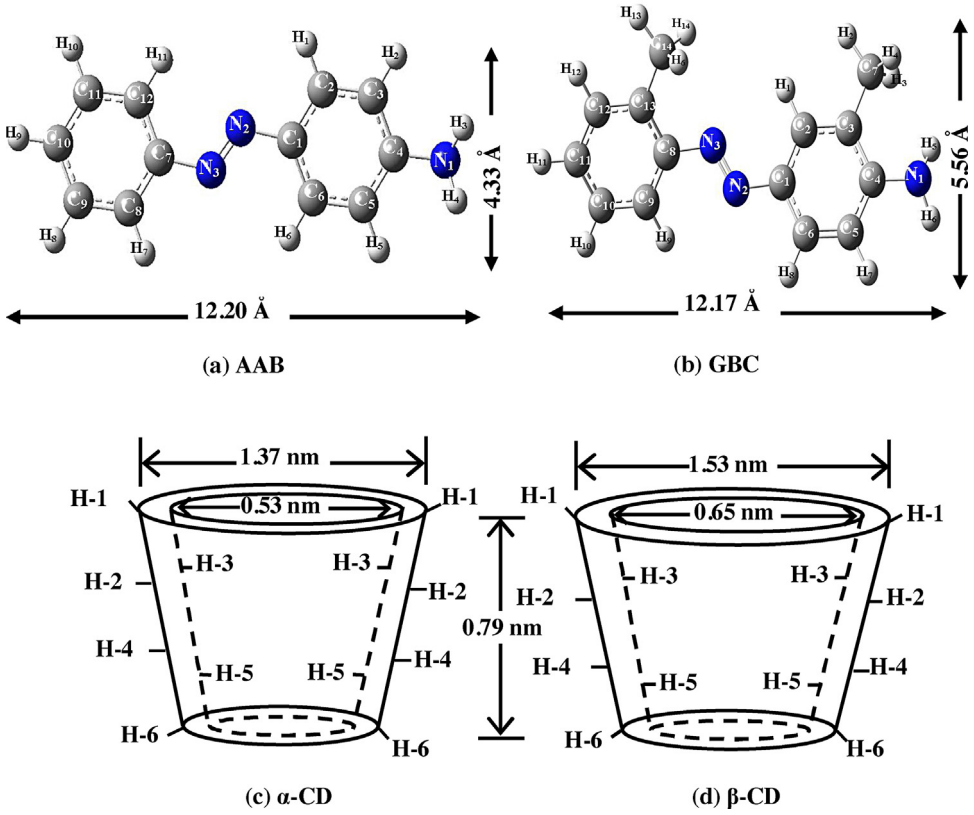

Fig. 1. The optimized structure with the numbering system of (a) AAB and (b) GBC obtained by PM3 level of theory and truncated cone shaped molecular structure of (c) α-CD and (d) β-CD.

method was proposed. The inclusion complexes were subsequently analyzed by absorption, fluorescence, fluorescence lifetime, FTIR, differential scanning calorimeter (DSC), powder X-ray diffraction (PXRD) and ^{1}H NMR techniques. The study of α-CD and β-CD with AAB and GBC is the extension of our earlier work (Antony Muthu Prabhu, Venkatesh, & Rajendiran, 2010; Antony Muthu Prabhu, Venkatesh, Sankaranarayanan, Siva, & Rajendiran, 2010; Premakumari et al., 2011; Venkatesh, Antony Muthu Prabhu, & Rajendiran, 2011).

2. Experiments

2.1. Reagents and materials

AAB, GBC, α-CD and β-CD were purchased from Sigma–Aldrich chemical company and used without further purification. Triply distilled water was used for the preparation of aqueous solutions. All solvents were used of the highest grade (spectrograde) and all the spectral measurements were performed at the solute concentrations of 2×10^{-5} M. The concentration of α-CD and β-CD solutions was varied from 1×10^{-3} to 10×10^{-3} M.

2.2. Preparation of nanomaterials

The α-CD or β-CD (1 mmol) was dissolved in 40 ml distilled water and AAB or GBC (1 mmol) in 10 ml methanol was slowly added to the CD solution. This mixture was sonicated at 40 °C for 2 h. Then the solution was refrigerated overnight at 5 °C. The precipitated AAB/CD and GBC/CD inclusion complexes were recovered by filtration and washed with little amount of ethanol and water to remove uncomplexed dyes and CDs, respectively. This precipitate was dried in vacuum at room temperature for two days and stored in an airtight bottle. These powder samples were used for further analysis.

2.3. Instruments

Absorption spectral measurements were carried out with a Shimadzu (Model UV 2600) UV–visible spectrophotometer and steady-state fluorescence measurements were analyzed using a Shimadzu spectrofluorimeter (Model RF-5301). The fluorescence lifetime measurements were performed using a picosecond laser and single photon counting setup from Jobin-Vyon IBH. Scanning electron microscopy (SEM) photographs were collected on a JEOL JSM 5610LV instrument. The morphology of AAB and GBC dyes encapsulated with CD inclusion complexes was investigated by TEM using a TECNAI G2 microscope with accelerating voltage 100 kV and 200 kV, using carbon coated copper TEM grid (200 mesh). FT-IR spectra of AAB, GBC, α-CD, β-CD and the inclusion complexes were measured between wave numbers 4000 cm^{-1} and 400 cm^{-1} on Nicolet Avatar 360 FT-IR spectrometer using KBr pellets. One-dimensional ^{1}H NMR spectra were recorded on a Bruker Avance 400 MHz spectrometer using DMSO-d_6 (99.9%) as a solvent. The DSC was recorded using Mettler Toledo DSC1 fitted with STR^e software, temperature scanning range was from 25 to 250 °C with a heating rate of 10 °C/min. PXRD spectra were recorded with a Bruker D8 advance diffractometer and the pattern was measured in the 2θ angle range between 5° and 80° with a scan rate 5°/min.

2.4. Molecular modeling studies

The theoretical calculations were performed using Gaussian 09 W. The initial geometries of the dye and CD molecules were constructed with Spartan 08 and then optimized by the PM3 method. α-CD and β-CD were fully optimized by PM3 without any

symmetry constraints (Antony Muthu Prabhu et al., 2012; Castro et al., 1996; Karelson, Lobanov, & Katrizky, 1996; Morokuma, 1977; Steiner & Koellner, 1994). Because the semiempirical PM3 method has been shown a powerful tool in the conformational study of CD complexes and has a high computational efficiency in calculating CD systems (Antony Muthu Prabhu et al., 2012; Castro et al., 1996; Karelson et al., 1996; Morokuma, 1977), it was selected to study the inclusion process of the CD with AAB and GBC in this work.

The glycosidic oxygen atoms of CD were placed onto the *XY* plane and their center was defined as the center of the coordination system. The primary hydroxyl groups were placed pointing toward the positive *Z* axis. The inclusion complexes were constructed from the PM3-optimized CD and guest molecules. The longer dimension of the guest molecule was initially placed onto the *Z* axis. The position of the guest was determined by the *Z* coordinate of one selected atom of the guest. The inclusion process was simulated by putting the guest in one end of CD and then letting it pass through the CD cavity. Since Density Functional Theory (DFT) calculations are expensive (cost and takes long time) in treating such large molecular systems, we used single point energy calculations to the PM3 optimized geometries using semiempirical method as implemented in Gaussian 03W.

For the construction of guest/CD complex, the glycosidic oxygen atoms of the cyclodextrin molecule were placed on the *XY* plane and their center was defined as the center of the coordinate system. The secondary hydroxyl groups of the CD were placed pointing toward the positive *Z* axis. The aromatic ring or the functional group of the guest molecule was initially placed along the *Z* axis. Two possible orientations of the guest molecules in the complex were considered. The orientation in which the aromatic ring of the guests points toward the primary hydroxyl of CD were called the "A orientation", or the other, in which the functional group (amino/hydroxyl/methoxy) of the guest points toward secondary hydroxyl of CD called the "B orientation" (Fig. S1).

The relative position between the host and the guest was measured by the *Z*-coordinate of the guest. The inclusion process emulation was then achieved along the *Z* axis from −10 to 10 Å with a step of 1 Å. The generated structures at each step were optimized by PM3 method without imposing any symmetrical restriction (Fig. S1).

3. Results and discussion

3.1. Absorption and emission spectroscopy

Absorption and emission spectra of GBC and AAB aqueous solutions containing different concentrations of α-CD and β-CD were shown in Table 1, Figs. S2 and S3. With an increasing CD concentration no marginal spectral shift is observed in the absorption spectra (GBC/AAB: λ_{abs} ~380 nm). The fluorescence spectra of azo molecules are more sensitive than the absorption spectra. As the CD concentration is increased, the fluorescence maximum is red shifted and the emission intensity increased along with CD concentrations. Such changes in absorption and emission spectra indicated that both molecules are caused by the introduction of CDs and that there is a formation of an inclusion complex.

The binding constant (*K*) value for GBC is higher than that of AAB, which can be attributed to the hydrophobic interaction between the phenyl ring (having the methyl group) and the internal wall of CD. Also, the higher *K* value of GBC shows that the fragment of phenyl group having the methyl substituent is too large to pass through the CD cavity. The *K* values also suggest that the steric hindrance of the methyl group prevents deep penetration and the fitness of the phenyl ring with azo group in the CD cavity better than that of AAB. The lower binding constant for AAB implies that the phenyl ring is not tightly embedded in the CD cavity. The ΔG values are negative, which suggest that the inclusion process proceeds spontaneously at room temperature.

The increase in fluorescence intensity of GBC/AAB molecules along with a large bathochromic shift (AAB: 424–456 nm; GBC: 430–455 nm) in CD as compared to that in aqueous solution may explained as follows: GBC/AAB molecules are embedded in two CD cavities in different directions to form the head-to-head dimer arrangement (i.e., barrel type). This unusual dimerization behavior is attributed to the cooperative interactions of hydrogen bonds between the secondary hydroxyl groups of two adjacent CD units as well as the π–π^* interaction between the benzene rings (Liu, Zhao, Chen, & Guo, 2005). Apart from that in aqueous solution, both isolated dyes show a clear yellow color; however, after adding of CDs, the color changed to yellow to orange, associated with increasing absorption band and red shifting of the emission band. The color changes may be induced by the strong binding of dyes into the CDs cavities.

3.2. Excited singlet state life time analysis

The lifetimes of the AAB and GBC dye molecules were measured in water and 0.01 M CD concentration of different CDs (Table S1). The excitation wavelength ($\lambda_{excitation}$) is 370 nm and emission wavelength ($\lambda_{emission}$) is 450 nm for AAB and GBC respectively. A total of 10,000 counts were collected for each sample. The decay curve might be fitted to three exponential functions for aqueous and CD media. However, it was observed that the three components of lifetime increased with decreasing polarity. This is due to the dye molecules encapsulated in to CD nano cavity. Both CD solutions τ_1 indicate a certain number of molecules remain uncomplexed with CD.

The short lifetime of AAB and GBC in absence of CD (water) is attributed to monomer of dyes and middle one is attributed to various hydrogen bonding interactions and longer one is attributed to the possible aggregates of AAB and GBC dyes. However, in CD medium, the shorter lifetimes are attributed to the three species of AAB and GBC, middle is due to hydrogen bonding and the longer one corresponds to the inclusion complex formation. Further, both the AAB and GBC can induce α-CD and β-CD to form nanostructures; hence, the fluorescence lifetime of AAB, GBC in α-CD nanocavity was longer than that of β-CD nanocavity. The higher life time of CD medium corresponds to a higher ordered structure of 2:2 complexes, possibly an extension of nanorod.

3.3. Molecular modeling studies

As described above, interactions between the AAB, GBC and CDs were studied experimentally which provided evidence for the formation of inclusion complexes (Antony Muthu Prabhu et al., 2012; Hihara, Okadab, & Morita, 2003; Sivasankar et al., 2012). For further confirmation, the geometries and stabilities of the inclusion complexes, as well as the formation of the lower energies (1:1) inclusion complexes were studied by theoretical method. The isolate and complex form of optimized structures of AAB and GBC is shown in Figs. 1 and S4. The binding energies are negative which express that the inclusion process of AAB and GBC in both CDs were thermodynamically stable. Compared to α-CD, the β-CD complex binding energy was more negative which indicated β-CD complex was more stable than α-CD complex (Table 2).

The aniline ring of the AAB and GBC deeply enters into the CD cavity and approaches the primary hydroxyl rim of the CD. The amino group of AAB and GBC readily form hydrogen bonds with hydroxyl groups of the CD edges and thus stabilizes the inclusion

Table 1
Absorption and fluorescence maxima of AAB with different α-CD and β-CD concentrations.

Concentration of CD (M)	AAB						GBC					
	α-CD			β-CD			α-CD			β-CD		
	λ_{abs}	Log ε	λ_{flu}	λ_{abs}	log ε	λ_{flu}	λ_{abs}	Log ε	λ_{flu}	λ_{abs}	Log ε	λ_{flu}
0 (without CD)	380 242	4.41 4.20	424	380 242	4.41 4.20	424	380 248	4.42 4.21	430	380 248	4.42 4.21	430
0.002	381 242	4.43 4.21	450	382 248	4.47 4.30	456	380 248	4.45 4.29	442	381 249	4.44	455
0.01	382 246	4.50 4.38	452	382 253	4.52 4.55	456	381 247	4.48 4.56	445	381 247	4.48 4.56	455
Excitation wavelength (nm)			370			370			370			370
K (1:1) M^{-1}	470		519	508		672	586		702	644		855
ΔG (kcal mol^{-1})	−3.70		−3.76	−3.74		−3.91	−3.83		−3.89	−4.24		−4.29

complexes. The hydrogen bond formation was one of the main driving forces for the complex formation in association with the hydrophobicity of CD cavity. The inner cavity of CD was not totally hydrophobic; rather, its polarity was similar to that of alcoholic solution.

The selected geometrical parameters, such as bond distance, bond angles, dihedral angles and hydrogen bond distances of AAB and GBC before and after complexation with CDs are shown in Table S2. From Fig. S4 it can be observed that the AAB and GBC molecules are partially positioned in the CD cavity. Further, the intermolecular H-bond is defined as O—H···N or N—H···O with the distance being greater than 2.5 Å. In all the complexes, the amino group of hydrogen has been bonded with the oxygen atom of primary hydroxy group of CD in the distance less than 3.00 Å.

The dipole moment of the AAB and GBC is lower than those of their respective complexes indicates the polarity of the CD cavity is altered after the guest enters into the cavity. The decrease in the dipole moment by increasing the binding energy implies that the dipole–dipole interactions are the main contribution to stabilize the AAB and GBC complex.

The energies of the HOMO and LUMO of the AAB and GBC, α-CD, β-CD and their inclusion complexes are summarized in Table 2. AAB and GBC molecules 3D plots of the frontier orbitals in the ground state HOMO and LUMO are shown in Fig. S5. From Table 2, it can be observed that the energy gap of the complex is lower than that of isolated dyes. This is made by the stabilization effect of the CD molecule. This implies that there is no notable change in the electronic spectrum of the AAB and GBC molecules during molecular encapsulation and binding.

3.4. Thermodynamic parameters

To examine the thermodynamics of the binding process, the statistical thermodynamic calculations were carried out at 1 atm pressure and 298.15 K temperature and the results are shown in Table 2. The positive Gibbs free energy changes ($\Delta G > 0$) for the α-CD complexes reveal that the formation of these inclusion complexes was arisen non-spontaneously, and the negative ΔG for the β-CD indicated that the complexes formation occurred spontaneously. The binding of AAB and GBC molecules with α-CD and β-CD are enthalpy–entropy co-driven process screening negative ΔH and ΔS values. The small negative $\Delta S < 0$ values are assumed to be due to augmentation of disorder in the scheme. The inclusion complexes showed the aniline ring with azo group completely entrapped inside the CD cavity (Fig. S4) and interact through hydrophobic interactions. Further, the slight negative ΔH ($\Delta H < 0$) values can be elucidated by the occurrence of hydrophobic interactions.

The difference in positive and negative ΔG values can be explained by the solvent effect. The experiments were conducted in aqueous medium and the computational work was done in vacuum phase. We were unable to do the computational work at the aqueous medium due to system limitations. Unfortunately because of the limitations in the calculation ability of the computer and the

Table 2
Energetic features, thermodynamic parameters and HOMO–LUMO energy calculations for AAB, GBC and its inclusion complexes by PM3 method.

Properties	AAB	GBC	α-CD	β-CD	AAB/α-CD	AAB/β-CD	GBC/α-CD	GBC/β-CD
E_{HOMO} (eV)	−8.58	−7.87	−10.37	−10.35	−8.41	−8.10	−7.69	−7.42
E_{LUMO} (eV)	−0.74	−0.63	1.26	1.23	−0.90	−0.57	−0.61	−0.62
E_{LUMO}–E_{HOMO} (eV)	7.84	8.5	11.63	11.58	7.51	7.53	7.08	8.04
μ	−4.66	−4.25	−4.56	−4.56	−4.65	−4.33	−4.15	−4.02
η	3.92	3.62	5.81	5.79	3.75	3.76	3.54	3.4
ω	2.77	2.49	1.78	1.79	2.88	2.49	2.43	2.37
S	0.25	0.27	0.17	0.17	0.26	0.26	0.28	0.29
Dipole moment (D)	1.51	1.70	11.34	12.29	6.81	11.58	7.44	10.01
E^a	87.83	72.50	−1247.62	−1457.63	−1168.52	−1379.88	−1181.89	−1397.82
ΔE^a					−8.73	−10.08	−6.77	−12.69
G^a	190.84	207.65	−676.37	−789.52	−477.72	−599.57	−452.10	−582.79
ΔG^a					7.81	−0.89	16.61	−0.92
H^a	226.01	247.41	−570.84	−667.55	−353.98	−457.31	−327.45	−434.87
ΔH^a					−9.15	−15.77	−4.02	−14.73
S^b	0.117	0.133	0.353	0.409	0.414	0.476	0.418	0.484
ΔS^b					−0.056	−0.050	−0.068	−0.047
ZPVE[a]	129.53	164.63	635.09	740.56	766.35	871.34	802.57	907.36

ZPVE – zero point vibrational energy.
[a] kcal mol^{-1}.
[b] kcal mol^{-1} K^{-1}.

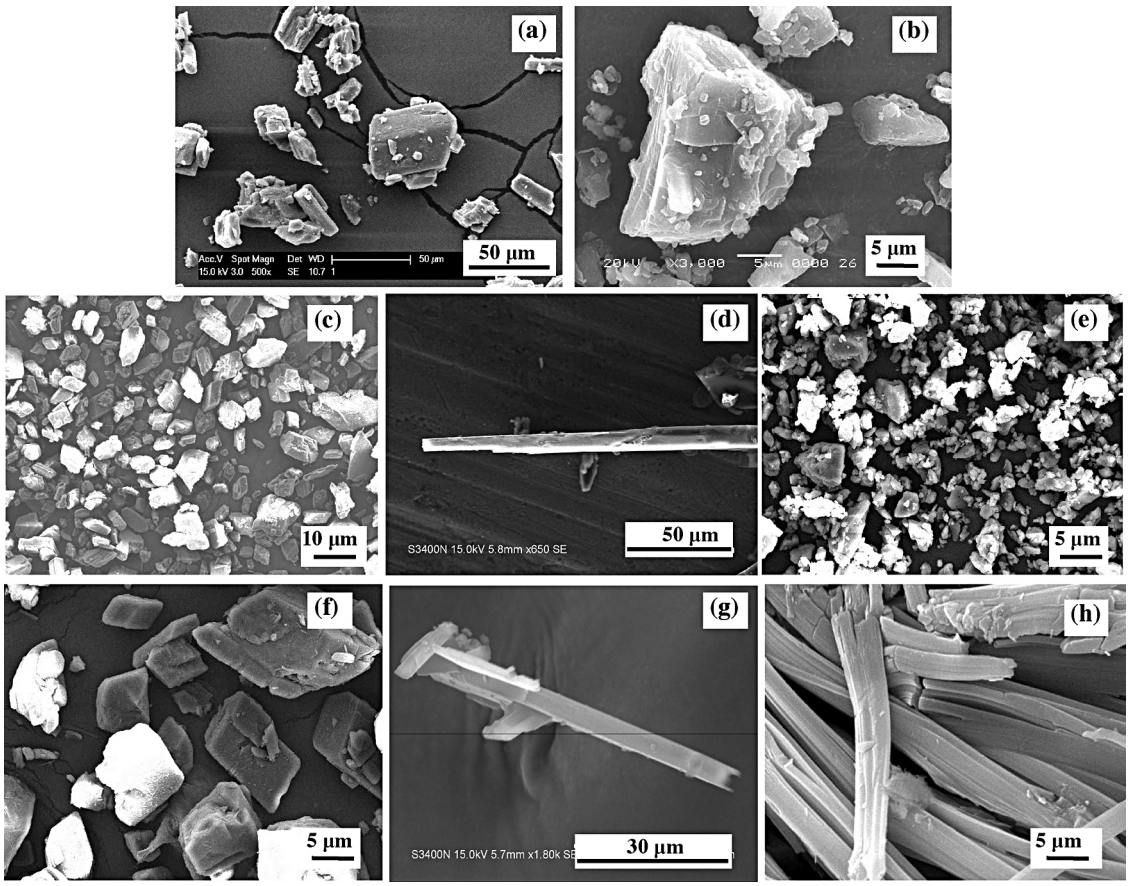

Fig. 2. SEM photographs of (a) α-CD, (b) β-CD, (c) AAB, (d) AAB/α-CD, (e) AAB/β-CD, (f) GBC, (g) GBC/α-CD and (h) GBC/β-CD.

large molecular size of CDs, calculations for these systems could not be performed for aqueous solutions and excited state. However, it is observed that the solvent effect on the host–guest interactions easily changes the inclusion reaction from a non-spontaneous process in the gas phase to a spontaneous one in the aqueous phase. The host–guest interaction causes an enthalpy–entropy compensating process in the gas phase whereas the same interaction causes an enthalpy–entropy co-driven process in aqueous solution, due to release of number of water molecules from the cavity of the CDs in inclusion complexation.

3.5. Nanomaterial observations

SEM images clearly show the difference in each case, α-CD has prismatic and β-CD has sheeted and platted form of appearance, whereas AAB and GBC dyes have stone rock structures. The evaluation of morphology revealed that, the inclusion complex was structurally dissimilar from the isolated components of dyes and CDs (Fig. 2). AAB/β-CD was observed as crystal structure, whereas, AAB/α-CD, GBC/α-CD and GBC/β-CD existed in micro level needle and rod resembling structures.

Size, shape, composition and material properties are extremely important parameters to construct the self-assembly nanostructures. TEM measurements were accomplished to determine the dimension and morphology of different nanostructures (nanorod, nanowire). The TEM image of AAB/α-CD, AAB/β-CD, GBC/α-CD and GBC/β-CD is shown in Fig. 3. The average thickness for AAB/CD nanorods was approximately in the range 10–55 nm, we observed that the nanorods are smooth surface and the corner was more sharp, whereas the GBC/CD nanostructure has different morphology i.e., nanowire, nanorod and agglomerated structures. The typical average dimension of GBC/α-CD: ±65–55 nm width and ~3 μm length, the 3D view of GBC/β-CD: ~200 nm thickness, ~75 nm width and ~1.6 nm length. The formation of ideal nanostructures is controlled by steric hindrance.

We proposed pseudorotaxane mechanism for the growth of the nanostructures. Both CD cavity internal distribution would agree to a dye bound with CD cavity to form energetic 1:1 (host:guest) inclusion complexes, then developed into a higher order 2:2 (host:guest) "barrel" type of inclusion complexes. Both nanostructures suggest that the individual "barrel" type (head to head arrangement) of 2:2 inclusion complexes form a various dimension of nanorods based on supramolecular pseudorotaxane mechanism. Earlier, we have shown that the host (β-CD) is a very adaptable system that exhibits AAB and GBC (guest) inclusion behavior of 2:2 complexes (Antony Muthu Prabhu, Venkatesh, & Rajendiran, 2010; Antony Muthu Prabhu, Venkatesh, Sankaranarayanan, et al., 2010). The significant torsional angle flexibility of the —N=N— group may be weak H-bonded with which the host assembles and binds the guest molecules in solid nanomaterials. Liu et al. (2005) reported that a linear structure was attained from 4-hydroxyazobenzene and 4-aminoazobenzene with β-CD complex by the intra- and inter-dimer hydrogen bonding, intradimer π–π interactions and wave-type structure were attained, respectively.

In a pseudorotaxane mechanism, there is no massive end group in both complexes (2:2 barrel type). Such type of barrel arrangement is self-assembled into a (AAB/CD, GBC/CD) different dimension of nanorod which may possibly form a single line head to head arrangement of 2:2 inclusion complex (Fig. 4). To understand the mechanism of nanorod arrangement, it is essential to design and tailor nanostructures. As like monomers to polymer

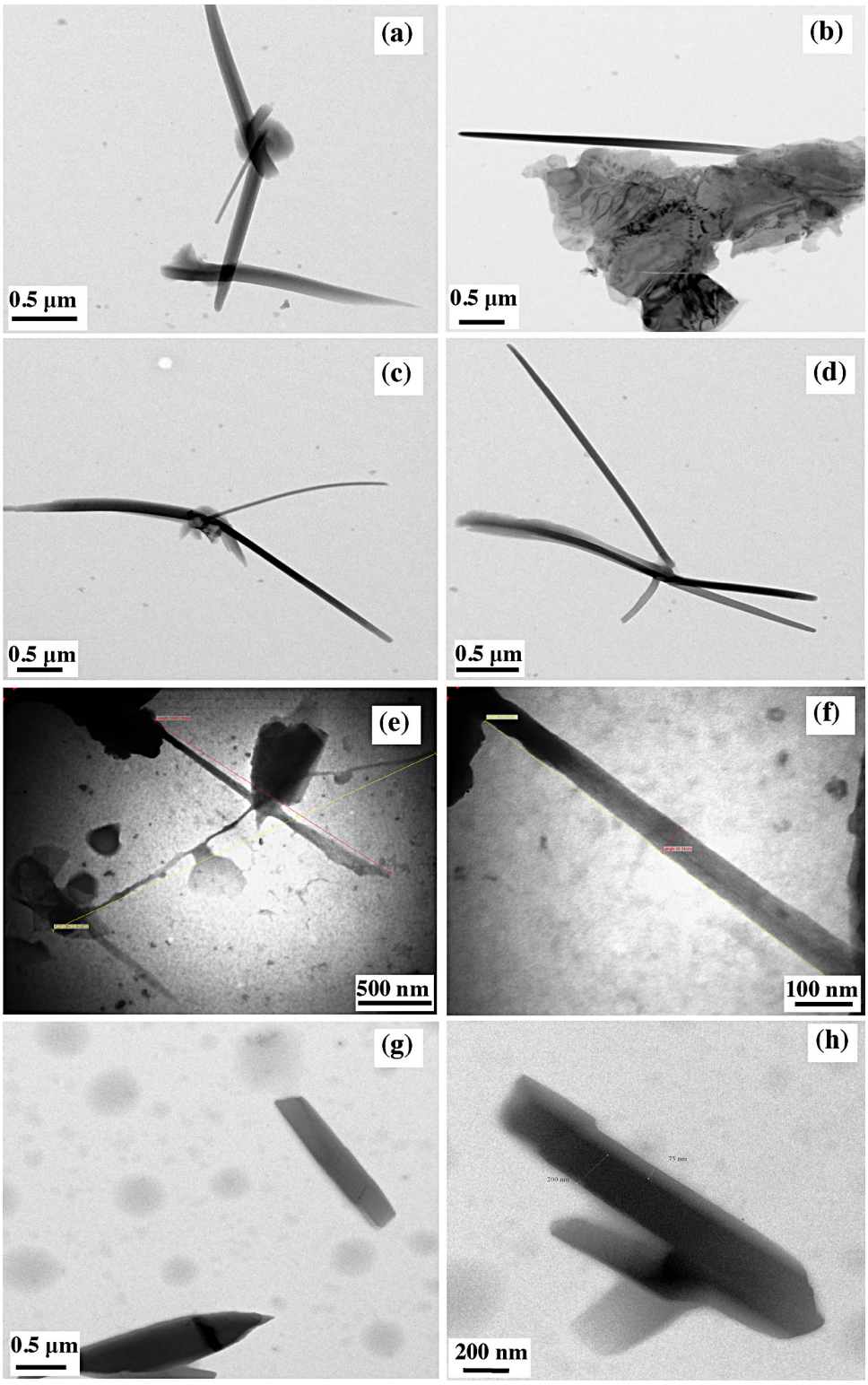

Fig. 3. TEM images of AAB/α-CD (a, b), AAB/β-CD (c, d), GBC/α-CD (e, f) and GBC/β-CD (g, h).

formation, the inclusion complex units were constructed the tiniest (single) nanorods through the tail to tail arrangement. The small individual nanorods are adjacently arranged through secondary self-assembly of CD hydroxyl group. The high order 2:2 complexes have confirmed the most versatile and successful approach to obtain linear CD pseduopolyrotaxanes. The length of the nanorod determines the length of the pseudopolyrotaxane (Harada, Li, & Kamachi, 1994a, 1994b; Saenger, 1984; Wenz & Keller, 1992). The guest with narrow molecular CD distributions are offered for the self-assembly of well-defined 2:2 inclusion complex. The above sequence can be retained by subsequent threading of different 2:2 complexes. Further, the key to the manipulation of the nano scale pseudorotaxane structure is believed to be related to various forces and hydrogen bonding. The development of nanostructures

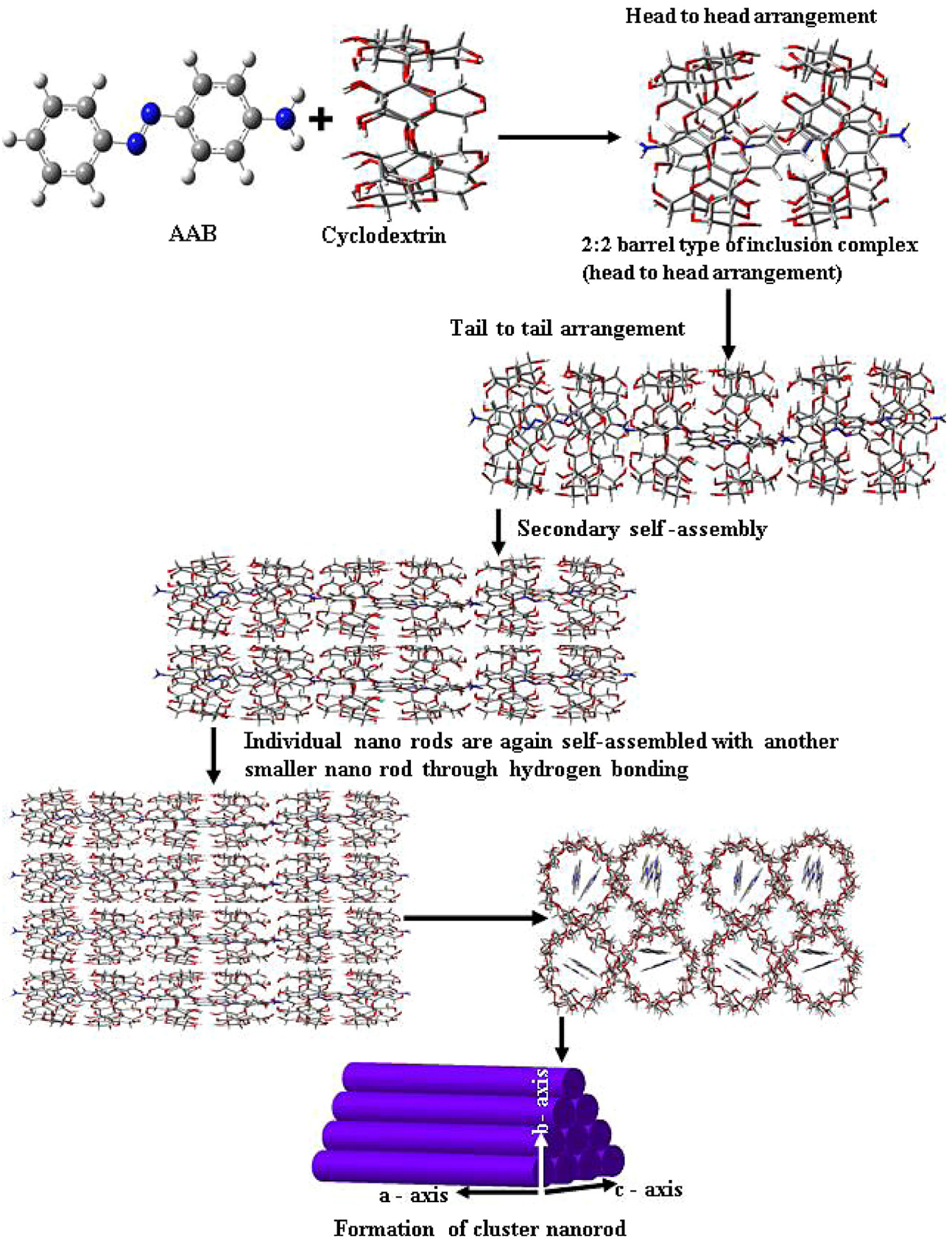

Fig. 4. Schematic representation of formation of micro rod and nanorod from inclusion complex.

is attributed to the following inter and intra molecular forces i.e., hydrogen bonding, hydrophilic and hydrophobic environment, weaker supramolecular interaction, van der Waals force and weaker assembly between the inclusion complexes of AAB and GBC with CDs (He, Fu, Shen, & Gao, 2008; Nepogodiev & Stoddart, 1998; Pistolis & Malliaris, 1996, 1998; Raymo & Stoddart, 1999).

To find out a number of AAB/CD or GBC/CD molecular level, smaller rods make up the three dimensional (3D) nanorods, we performed molecular modeling studies on the individual AAB/CD or GBC/CD inclusion complex. From the molecular modeling studies, a single AAB/CD and GBC/CD inclusion complex height is 17.55 Å (1.755 nm), thickness of α-CD and β-CD complexes are 14.2 Å (1.42 nm) and 15.7 Å (1.57 nm) respectively. Initially ~295–1766 units of AAB/α-CD form a different length (tiny and lengthy) of primary single nanorod (head to head arrangement) the consequences of such nanorod (*a*-axis) leads to the substantial growth of ~60–80 adjacent nanorods. This nanorods later arranged through secondary self-assembly along the 'b' axis (Fig. 4). This arrangement terminates with the formation of ~40–80 nm thickness of many nanorods. The GBC/β-CD complex shows the 3D dimensional bulk nanorod and other nanorods. The number of ~683 units of GBC/β-CD grows primary single nanorods (~1200 nm). Such a nanorod (a-axis) leads to the considerable growth of ~35–50 numbers of adjacent nanorods formed over the secondary self-assembly of single layer by the way of '*b*' axis. Further, the single layer developed along with '*c*' axis by stacking force which leads to the formation of 3D nanorod structure.

3.6. FTIR spectra analysis

The FTIR spectra of α-CD, β-CD, AAB, GBC and the solid inclusion complexes are shown in Figs. S6 and S7. In comparison of AAB, GBC, α-CD and β-CD the CH stretching vibrations at 2923, 2840 cm^{-1} and 2923, 3198 cm^{-1} are largely shifted (~5 cm^{-1}) to longer frequency in the inclusion complexes. In the inclusion complex, the C=C stretching vibration at ~1620 cm^{-1} is slightly moved to longer frequency. The frequencies appeared at 3468, 3380 cm^{-1} and 3489, 3364 cm^{-1} are assigned to the aromatic amino stretching vibration of isolated AAB and GBC molecules, moved to lower frequencies at 3415, 3397 cm^{-1} and 3380 cm^{-1} and 3376 cm^{-1} for both α-CD and β-CD inclusion complexes, respectively. The stretching vibrations at 564, 546 cm^{-1} are due to the ring deformation stretching of the AAB and GBC molecules and it moved to a longer frequency (~20 cm^{-1}) in the inclusion complexes. Further, the AAB and GBC, the amino group deformation, which appear at 1620 and 1593 cm^{-1} are shifted in the complex to 1630 and 1599 cm^{-1} respectively. Moreover, the azo group stretching frequency intensities of AAB and GBC at 1502–1414 cm^{-1} and 1500–1396 cm^{-1} are strongly affected in the inclusion complexes indicating azo group is included in the CD cavities.

3.7. Differential scanning calorimetry analysis

DSC analysis has been shown to be a powerful analytical tool to analyze the interactions between guest and host molecules. The DSC curve of α-CD and β-CD shows a broad endothermic peak around 78.8 °C, 108.5 °C, 135.4 °C and 128.0 °C respectively (Fig. 5). These endothermic peaks are associated with water loss of the crystal (Figueiras, Carvalho, Ribeiro, Torres-Labandeira, & Veiga, 2007; Rekhasky & Inoue, 1998). The sharp melting point curve of AAB, GBC appeared at 123.6 °C and 100.1 °C respectively. Further the endothermic transition of AAB/CD and GBC/CD are distinctly changed in both isolated α-CD and β-CD. The change of the endothermic transition could provide evidence for the complex formation comparison of isolated component.

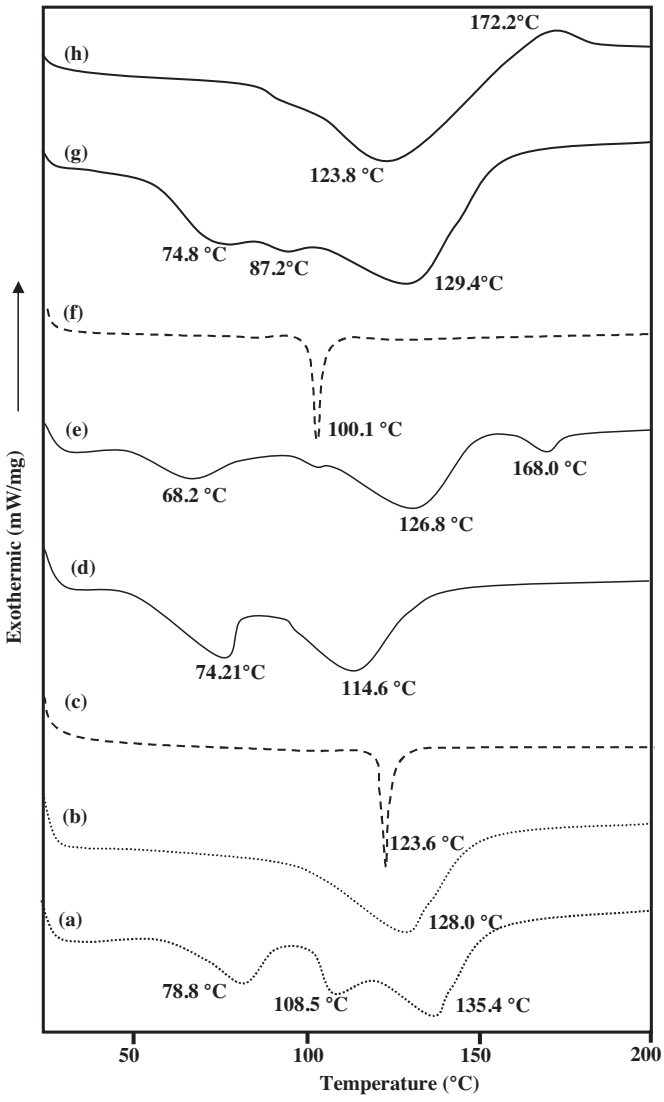

Fig. 5. DSC curves of (a) α-CD, (b) β-CD, (c) AAB, (d) AAB/α-CD, (e) AAB/β-CD, (f) GBC, (g) GBC/α-CD and (h) GBC/β-CD 1:1 inclusion complexes.

Moreover, the shape of the endothermic transition curve is attributed to dehydration of CD cavity. The cited changes of thermal property and disappearance of both guest melting events would indicate the complex formation.

3.8. Powder X-diffraction analysis

Powder XRD patterns permit the evaluation of the average and extensive range ordering of materials (Correia et al., 2002). The diffraction pattern of the complex is understood to be separate from that of the superposition of each of the components while a real host:guest inclusion complex is formed (Veiga, Teixeira-Dias, Kedzierewicz, Sousa, & Maincent, 1996). The powder XRD patterns of α-CD, β-CD, AAB, GBC, and their inclusion complex are shown in Fig. 6. The XRD pattern of all isolated components displays the sharp peaks in the 10°–30° (2θ) range, thus proving the crystalline character of these isolated compounds. Meanwhile, the XRD pattern of α-CD, β-CD, AAB, GBC illustrates intense, sharp peaks for α-CD at 11.94°, 14.11°, 21.77° for β-CD at 11.49°, 17.58°; for AAB at 16.63° and GBC at 11.58°, 13.68°, 18.23°, 22.92°, 25.38° as well as several minor peaks were observed in CDs and dyes. These peaks prove the crystalline character of the isolated system. In the XRD pattern, the selected peak for the inclusion complexes was given

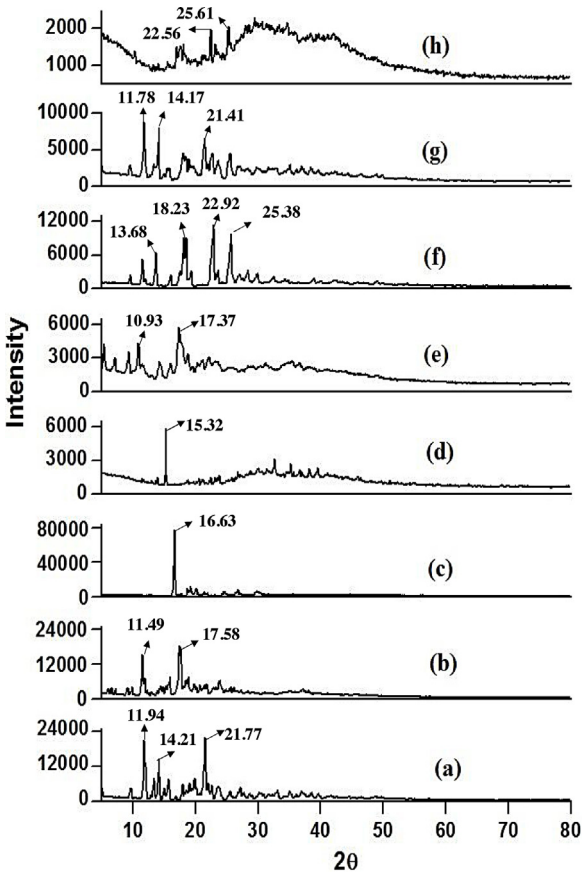

Fig. 6. Powder X-ray diffractograms of inclusion (a) α-CD, (b) β-CD, (c) AAB, (d) AAB/α-CD. (e) AAB/β-CD, (f) GBC, (g) GBC/α-CD and (h) GBC/β-CD 1:1 inclusion complexes.

below: AAB/α-CD: 15.32°, 32.71°, 35.23°; AAB/β-CD: 5.36°, 9.32°, 10.93°, 17.37°; GBC/α-CD: 11.78°, 14.17°, 21.41°, 22.65°, 25.61°; GBC/β-CD: 18.30°, 22.56°, 25.24°. The patterns of complexes suggest a decrease in the crystallinity as result of the formation of inclusion complex.

3.9. NMR analysis

Proton nuclear magnetic resonance (^{1}H NMR) spectroscopy has proved to be a powerful tool in the study of inclusion complexes. ^{1}H NMR spectroscopy provides an effective means of assessing the dynamic interaction site of CDs with that of the guest molecules. The basis of information gained from NMR spectroscopy is located in this shifts, loss of resolution and broadening of signals observed for the host and guest protons. The resonance assignments of the protons of the CDs are well established and contain six varieties of protons. In β-CD, H_1 doublet appears at δ 5.06 ppm, H_3 triplet appears at δ 3.94 ppm and a strong unresolved broad peak consisting of δ H_5 and δ H_6 appears at δ 3.87–3.85 ppm. H_2 protons appearing as two doublets centered at δ 3.64 ppm and δ 3.67 ppm and H_4 triplet appears at δ 3.58 ppm. The chemical shifts of CD protons reported by different authors (Rekhasky & Inoue, 1998) are very close to those reported in this work. The H-3 and H-5 protons are placed in the interior hydrophobic part of the CD cavity; hence the interaction of the guest (AAB, GBC) with the inner CD cavity affects the chemical shifts of the H-3 and H-5 protons (Fig. S7). A minor shift is observed for the H-1and H-6 protons, located on the edge of the CD cavity (Rekhasky & Inoue, 1998). These protons are involved in intermolecular hydrogen bond between the complex or CDs and possibly a head to head or tail to tail arrangement through self-assembly of the complex.

AAB/α-CD complex/β-CD complex: H_a-7.690/7.754/7.747; H_b-7.646/7.684/7.674; H_c-7.454/7.508/7.531; H_d-7.385/7.431/7.436; H_e-6.690/6.697/6.684; H_f-5.873/5.592/5.710.

GBC/α-CD complex/β-CD complex: H_a-7.546/7.621/7.702; H_b-7.410/7.481/7.567; H_c-7.324/7.501/7.480; H_d-7.277/7.311/7.355; H_e-7.240/7.289/7.316; H_f-6.721/7.729/6.725; H_g-5.568/5.769/5.820; H_j-4.133/4.482/4.83; H_k-2.541/2.600/2.599, H_m-2.103/2.193/2.138.

It can be seen from the above results, the chemical shifts data for the inclusion complex were different from that of the free compound. In AAB, compared to other protons a large down field chemical shift observed in the H_a, H_c, H_e and amino protons indicates that both aromatic rings are deeply entrapped in the CD cavity. In GBC, a large down field chemical shift observed in the H_b, H_c, H_f, H_g, H_j and H_m protons indicates that both aromatic rings are deeply entrapped in the CD cavity. The chemical shift values of amino protons are highly shifted to down field in the complex: AAB/α-CD ∼ −0.5 ppm and AAB/β-CD ∼0.16 ppm; GBC/α-CD ∼ −0.35 ppm and GBC/β-CD ∼ −0.7 ppm respectively as compared with corresponding free AAB, GBC molecule. These results indicated that the amino and aromatic part of both molecules interact strongly with CDs cavities.

4. Conclusions

AAB/CD and GBC/CD inclusion complex nanostructures (nanorod and nanowire) were arranged through self-assembly. It is observed that AAB with α-CD and β-CD shows nearly similar type of nanostructures, and the size of the CD cavity does not affect the formation and dimension of the nanostructure, whereas the GBC/CD shows the disparity nanostructures. The AAB/CD and GBC/CD nanostructures are formed from higher ordered head to head arrangement of 2:2 inclusion complexes. The encapsulation of azo dyes with CD cavities could lead to color change of the solution. This color change is expected to be due to the conformational changes of the dyes in hydrophobic CD cavity. Theoretical studies propose that hydrophobic interaction and hydrogen bonding play a significant role in determining the stability of the complexes.

Acknowledgements

This work is supported by the CSIR (No. 01(2549)/12/EMR-II) and UGC (F. No. 41-351/2012 (SR)). One of the authors R. K. Sankaranarayanan is thankful to CSIR, New Delhi for the award of Senior Research Fellowship. The authors acknowledge UGC Networking Resource Centre, School of Chemistry and Centre for Nanotechnology, University of Hyderabad for providing equipment facilities for characterization. We gratefully acknowledge Prof. M.V. Rajasekharan, Dean School of Chemistry, University of Hyderabad for his kind help. We thank Dr. P. Ramamurthy, Director, National Centre for Ultrafast Processes, University of Madras, for allowing the fluorescence lifetime measurements for this work.

Appendix A. Supplementary data

Supplementary data associated with this article can be found, in the online version, at http://dx.doi.org/10.1016/j.carbpol.2014.01.030.

References

Anconi, C. P. A., Nascimento, C. S., De Almeida, W. B., & Dos Santos, H. F. (2012). Theoretical study of covalently bound A-cyclodextrin associations. *Journal of Physical Chemistry C*, *116*, 18958–18964.

Antony Muthu Prabhu, A., Sankaranarayanan, R. K., Venkatesh, G., & Rajendiran, N. (2012). Dual fluorescence of fast blue RR and fast violet B: Effect of solvents, α- and β-cyclodextrins. *Journal of Physical Chemistry B*, *116*, 9061–9074.

Antony Muthu Prabhu, A., Venkatesh, G., & Rajendiran, N. (2010). Azo-hydrazo tautomerism and inclusion complexation of 1-phenylazo-2-naphthols with various solvents and β-cyclodextrin. *Journal of Fluorescence*, *20*, 961–972.

Antony Muthu Prabhu, A., Venkatesh, G., Sankaranarayanan, R. K., Siva, S., & Rajendiran, N. (2010). Azonium-ammonium tautomerism and inclusion complexation of 4-amino-2′,3-dimethylazobenzene. *Indian Journal of Chemistry*, *49A*, 407–417.

Castro, R., Berardi, M. J., Cordova, E., de Olza, M. O., Kaifer, A. E., & Evanseck, J. D. (1996). Unexpected roles of guest polarizability and maximum hardness, and of host solvation in supramolecular inclusion complexes: A dual theoretical and experimental study. *Journal of American Chemical Society*, *118*, 10257–10268.

Ceccato, M., Lo Nostro, P., & Baglioni, P. (1997). Alpha-cyclodextrin/polyethylene glycolpolyrotaxane: A study of the threading process. *Langmuir*, *13*, 2436–2439.

Connors, K. A. (1997). The stability of cyclodextrin complexes in solution. *Chemical Reviews*, *97*, 1325–1357.

Correia, I., Bezzenine, N., Ronzani, N., Platzer, N., Beloeil, J. C., & Doan, B. T. J. (2002). Study of inclusion complexes of acridine with β- and (2-6-di-O-methyl)-β-cyclodextrin by use of solubility diagrams and NMR spectroscopy. *Journal of Physical Organic Chemistry*, *15*, 647–659.

Figueiras, A., Carvalho, R. A., Ribeiro, L., Torres-Labandeira, J. J., & Veiga, F. J. B. (2007). Solid-state characterization and dissolution profiles of the inclusion complexes of omeprazole with native and chemically modified beta-cyclodextrin. *European Journal of Pharmaceutics and Biopharmaceutics*, *67*, 531–539.

Harada, A. (2001). Cyclodextrin-based molecular machines. *Accounts of Chemical Research*, *34*, 456–464.

Harada, A., Li, J., & Kamachi, M. (1994a). Double-stranded inclusion complexes of cyclodextrin threaded on poly(ethylene glycol). *Nature*, *370*, 126–128.

Harada, A., Li, J., & Kamachi, M. (1994b). Preparation and characterization of a polyrotaxane consisting of monodisperse poly(ethylene glycol). *Journal of American Chemical Society*, *116*, 3192–3196.

He, Y. F., Fu, P., Shen, X. H., & Gao, H. C. (2008). Cyclodextrin-based aggregates and characterization by microscopy. *Micron*, *39*, 495–516.

Hihara, T., Okadab, Y., & Morita, Z. (2003). Azo-hydrazone tautomerism of phenylazonaphthol sulfonates and their analysis using the semiempirical molecular orbital PM5 method. *Dyes and Pigments*, *59*, 25–41.

Karelson, M., Lobanov, V. S., & Katrizky, R. (1996). Quantum-chemical descriptors in QSAR/QSPR studies. *Chemical Reviews*, *96*, 1027–1044.

Liu, Y., Zhao, Y.-L., Chen, Y., & Guo, D. S. (2005). Assembly behavior of inclusion complexes of β-cyclodextrin with 4-hydroxyazobenzene and 4-aminoazobenzene. *Organic and Biomolecular Chemistry*, *3*, 584–591.

Madrid, J. M., Mendicuti, F., & Mattice, W. L. (1998). Inclusion complexes of 2-methylnaphthoate and gamma-cyclodextrin – Experimental thermodynamics and molecular mechanics calculations. *Journal of Physical Chemistry B*, *102*, 2037–2044.

Madrid, J. M., Pozuelo, J., Mendicuti, F., & Mattice, W. L. J. (1997). Molecular mechanics study of the inclusion complexes of 2-methyl naphthoate with α- and β-cyclodextrins. *Colloid Interface Science*, *193*, 112–120.

Miyake, K., Yasuda, S., Harada, A., Sumaoka, J., Komiyama, M., & Shigekawa, H. (2003). Formation process of cyclodextrin necklace-analysis of hydrogen bonding on a molecular level. *Journal of American Chemical Society*, *125*, 5080–5085.

Mohsen, T., & Mina, G. (2009). Structure and conformation of α-,β- and γ-cyclodextrin in solution: Theoretical approaches and experimental validation. *Carbohydrate Polymers*, *78*, 10–15.

Morokuma, K. (1977). Why do molecules interact? The origin of electron donor-acceptor complexes, hydrogen bonding and proton affinity. *Accounts Chemical Research*, *10*, 294–300.

Nepogodiev, S. A., & Stoddart, J. F. (1998). Cyclodextrin-based catenanes and rotaxanes. *Chemical Reviews*, *98*, 1959–1976.

Pistolis, G., & Malliaris, A. (1996). Nano tube formation between cyclodextrins and 1,6-diphenyl-1,3,5-hexatriene. *Journal of Physical Chemistry*, *100*, 15562–15568.

Pistolis, G., & Malliaris, A. (1998). Size effect of alpha, omega-diphenylpolyenes on the formation of nanotubes with gamma-cyclodextrin. *Journal of Physical Chemistry B*, *102*, 1095–1101.

Premakumari, J., Allan Gnana Roy, G., Antony Muthu Prabhu, A., Venkatesh, G., Subramanian, V. K., & Rajendiran, N. (2011). Effect of solvents and pH on β-cyclodextrin inclusion complexation of 2,4-dihydroxyazobenzene and 4-hydroxyazobenzene. *Journal of Solution Chemistry*, *40*, 327–347.

Rajendiran, N., & Siva, S. (2014). Inclusion complex of sulfadimethoxine with cyclodextrins: Preparation and characterization. *Carbohydrate Polymers*, *101*, 828–836.

Raymo, F. M., & Stoddart, J. F. (1999). Interlocked macromolecules. *Chemical Reviews*, *99*, 1643–1663.

Rekhasky, M. V., & Inoue, Y. (1998). Complexation thermodynamics of cyclodextrins. *Chemical Reviews*, *98*, 1875–1918.

Saenger, W. (1984). J. L. Atwood, J. E. K. Davies, & D. D. MacNicol (Eds.), *Inclusion compounds* (Vol. 2). London: Academic Press.

Sankaranarayanan, R. K., & Rajendiran, N. (2013). Nanorod formation of cyclodextrincovered sudan dyes through supramolecular self-assembly. *Journal of Experimental Nanoscience*, http://dx.doi.org/10.1080/17458080.2013.840934

Sherrod, M. J. (1992). In J. E. D. Davies (Ed.), *In spectroscopic and computational studies of supramolecular systems* (p. 187). Dordrecht, The Netherlands: Kluwer Academic Publishers.

Sivasankar, T., Antony Muthu Prabhu, A., Karthick, M., & Rajendiran, N. (2012). Encapsulation of vanillylamine by native and modified cyclodextrins: Spectral and computational studies. *Journal of Molecular Structure*, *1028*, 57–67.

Steiner, T., & Koellner, G. (1994). β-Cyclodextrin hydrate clathrate. *Journal of American Chemical Society*, *116*, 5122–5128.

Szejtli, J. (1998). Introduction and general overview of cyclodextrin chemistry. *Chemical Reviews*, *98*, 1743–1753.

VD'Souza, V. T., & Lipkowitz, K. B. (1998). Applications of computational chemistry to the study of cyclodextrins. *Chemical Reviews*, *98*(5), 1829–1874.

Veiga, F., Teixeira-Dias, J. J. C., Kedzierewicz, F., Sousa, A., & Maincent, P. (1996). Inclusion complexation of tolbutamide with β-cyclodextrin and hydroxypropyl-β-cyclodextrin. *International Journal of Pharmaceutics*, *129*, 63–71.

Venkatesh, G., Antony Muthu Prabhu, A., & Rajendiran, N. (2011). Azonium-ammonium tautomerism and inclusion complexation of 1-(2,4-diamino phenylazo) naphthalene and 4-aminoazobenzene. *Journal of Fluorescence*, *21*, 1485–1497.

Wenz, G., & Keller, B. (1992). Threading cyclodextrin rings on polymer chains. *Angewandte Chemie International Edition English*, *31*, 197–199.

Wu, A. H., Shen, X. H., & He, Y. K. (2006). Investigation on γ-cyclodextrin nanotube induced by N,N′-diphenylbenzidine molecule. *Journal of Colloidal Interface Science*, *297*, 525–533.